The Journal of Immunology

Resolvin D1 and Its Precursor Docosahexaenoic Acid Promote Resolution of Adipose Tissue Inflammation by Eliciting Macrophage Polarization toward an M2-Like Phenotype

Esther Titos, Bibiana Rius, Ana González-Périz, Cristina López-Vicario, Eva Morán-Salvador, Marcos Martínez-Clemente, Vicente Arroyo and Joan Clària

J Immunol 2011; 187:5408-5418; Prepublished online 17 October 2011;
doi: 10.4049/jimmunol.1100225
http://www.jimmunol.org/content/187/10/5408

The Journal of Immunology is published twice each month by
The American Association of Immunologists, Inc.,
1451 Rockville Pike, Suite 650, Rockville, MD 20852

Print ISSN: 0022-1767 Online ISSN: 1550-6606.

Resolvin D1 and Its Precursor Docosahexaenoic Acid Promote Resolution of Adipose Tissue Inflammation by Eliciting Macrophage Polarization toward an M2-Like Phenotype

Esther Titos,*,† Bibiana Rius,* Ana González-Périz,*,† Cristina López-Vicario,* Eva Morán-Salvador,* Marcos Martínez-Clemente,* Vicente Arroyo,†,‡ and Joan Clària*,†,§

We recently demonstrated that ω-3-polyunsaturated fatty acids ameliorate obesity-induced adipose tissue inflammation and insulin resistance. In this study, we report novel mechanisms underlying ω-3-polyunsaturated fatty acid actions on adipose tissue, adipocytes, and stromal vascular cells (SVC). Inflamed adipose tissue from high-fat diet-induced obese mice showed increased F4/80 and CD11b double-positive macrophage staining and elevated IL-6 and MCP-1 levels. Docosahexaenoic acid (DHA; 4 μg/g) did not change the total number of macrophages but significantly reduced the percentage of high CD11b/high F4/80-expressing cells in parallel with the emergence of low-expressing CD11b/F4/80 macrophages in the adipose tissue. This effect was associated with downregulation of proinflammatory adipokines in parallel with increased expression of IL-10, CD206, arginase 1, resistin-like molecule α, and chitinase-3 like protein, indicating a phenotypic switch in macrophage polarization toward an M2-like phenotype. This shift was confined to the SVC fraction, in which secretion of Th1 cytokines (IL-6, MCP-1, and TNF-α) was blocked by DHA. Notably, resolvin D1, an anti-inflammatory and proresolving mediator biosynthesized from DHA, markedly attenuated IFN-γ/LPS-induced Th1 cytokines while upregulating arginase 1 expression in a concentration-dependent manner. Resolvin D1 also stimulated nonphlogistic phagocytosis in adipose SVC macrophages by increasing both the number of macrophages containing ingested particles and the number of phagocytosed particles and by reducing macrophage reactive oxygen species production. No changes in adipocyte area and the phosphorylation of hormone-sensitive lipase, a rate-limiting enzyme regulating adipocyte lipolysis, were observed. These findings illustrate novel mechanisms through which resolvin D1 and its precursor DHA confer anti-inflammatory and proresolving actions in inflamed adipose tissue. ***The Journal of Immunology*****, 2011, 187: 5408–5418.**

The presence of a chronic "low-grade" state of mild inflammation in adipose tissue is a hallmark of obesity. This subclinical inflammatory state plays a critical role in the development of obesity-associated complications such as insulin resistance, atherosclerosis, type 2 diabetes, and non-alcoholic fatty liver disease (1, 2). Recent studies have demonstrated that adipose tissue macrophages, which are a prominent source of proinflammatory adipokines such as TNF-α and IL-6, provide a causal link between obesity-induced adipose tissue inflammation and insulin resistance (3–5). Indeed, studies in both humans and rodents indicate that macrophages accumulate in adipose tissue with increasing body weight and their quantity correlates with measures of adipose tissue inflammation and insulin resistance (3–5). Consistently, weight loss leads to a reduction in both inflammatory markers and adipose tissue macrophage content (6).

Docosahexaenoic acid (DHA; C22:6n-3) is a typical long-chain polyunsaturated fatty acid (PUFA) of the ω-3 series that exerts unequivocal beneficial actions in several disease conditions. This ω-3-PUFA has been shown to be a safe and effective therapy and preventive strategy against obesity-related complications such as insulin resistance and hepatic steatosis in both obese subjects and animals (7–10). However, the scope and design of these studies did not allow the identification of the mechanisms implicated in the beneficial actions of ω-3-PUFAs. Recently, the understanding of the mechanisms underlying the recognized therapeutic values of ω-3-PUFAs has been challenged by the discovery of a novel family of endogenously generated autacoids, namely resolvins and protectins, with potent anti-inflammatory and proresolving activities (reviewed in Refs. 11, 12). Among this novel genus of anti-inflammatory and proresolving autacoids, resolvin D1 (7*S*,8*R*,17*S*-trihydroxy-docosa-4*Z*,9*E*,11*E*,13*Z*,15*E*,19*Z*-hexaenoic acid), which

*Department of Biochemistry and Molecular Genetics, Hospital Clinic, Center Esther Koplowitz, August Pi i Sunyer Biomedical Research Institute, 08036 Barcelona, Spain; †Biomedical Research Networking Center on Liver and Digestive Diseases, 08036 Barcelona, Spain; ‡Liver Unit, Hospital Clinic, Center Esther Koplowitz, August Pi i Sunyer Biomedical Research Institute, 08036 Barcelona, Spain; and §Department of Physiological Sciences I, University of Barcelona, 08036 Barcelona, Spain

Received for publication January 24, 2011. Accepted for publication September 10, 2011.

This work was supported by a grant from the Ministerio de Ciencia e Innovación (SAF 09/08767). The Biomedical Research Networking Center on Liver and Digestive Diseases is funded by the Instituto de Salud Carlos III. Our laboratory is a Consolidated Research Group recognized by the Generalitat de Catalunya (2009SGR1484). E.T. and A.G.-P. have contracts with the Biomedical Research Networking Center on Liver and Digestive Diseases. E.M.-S. was supported by the Ministerio de Ciencia e Innovación. C.L.-V. was supported by the August Pi i Sunyer Biomedical Research Institute.

Address correspondence and reprint requests to Prof. Joan Clària and Dr. Esther Titos, Department of Biochemistry and Molecular Genetics, Hospital Clinic, Center Esther Koplowitz, Villarroel 170, Barcelona 08036, Spain. E-mail addresses: jclaria@clinic.ub.es (J.C.) and esther.titos@ciberehd.org (E.T.)

Abbreviations used in this article: ALT, alanine aminotransferase; Arg1, arginase 1; b.w., body weight; CD206, mannose receptor C type 1; DHA, docosahexaenoic acid; FAF, fatty-acid free; HFD, high-fat diet; HSL, hormone-sensitive lipase; iNOS, inducible NO synthase; 5-LO, 5-lipoxygenase; 12/15-LO, 12/15-lipoxygenase; 15-LO, 15-lipoxygenase; PAI-1, plasminogen activator inhibitor-1; PPARγ, peroxisome proliferator-activated receptor γ; PUFA, polyunsaturated fatty acid; RELMα, resistin-like molecule α; ROS, reactive oxygen species; SVC, stromal vascular cells; TAG, triglycerides; Ym1, chitinase-3 like protein.

www.jimmunol.org/cgi/doi/10.4049/jimmunol.1100225

in humans originates from endogenous sources of DHA via 15-lipoxygenase (15-LO) and 5-lipoxygenase (5-LO) interactions [via 12/15-lipoxygenase (12/15-LO) and 5-LO interactions in mice], has been established to exert potent protective effects (13–16). Promotion of the timely resolution of inflammation and reduction of the magnitude of tissue injury are the most significant actions of resolvin D1 (14–16). Notably, among the anti-inflammatory lipid mediators, resolvin D1 largely predominates in adipose tissue from obese mice (7).

In the current investigation, we explored the mechanisms by which ω-3-PUFAs modulate the inflammatory status in adipose tissue from obese mice, with special emphasis on adipose tissue macrophages present in the stromal vascular cell fraction. The findings obtained in our experimental model of dietary obesity indicate that the ω-3-PUFA DHA induces a phenotypic switch in adipose tissue macrophages from a proinflammatory classical activation profile toward an alternatively anti-inflammatory M2-like state. This phenotypic switch was accompanied by inhibition of secreted proinflammatory adipokines in adipose tissue cells confined to the stromal vascular fraction. Importantly, we demonstrate that resolvin D1 is a local acting signal that exhibits robust anti-inflammatory properties in macrophages and promotes macrophage nonphlogistic phagocytosis, a critical step in the resolution of the inflammatory process.

Materials and Methods

Materials

DHA, arachidonic acid, and resolvin D1 (7*S*,8*R*,17*S*-trihydroxy-docosa-4*Z*,9*E*,11*E*,13*Z*,15*E*,19*Z*-hexaenoic acid) (13, 17), were from Cayman Chemicals (Ann Arbor, MI). Recombinant mouse IFN-γ and IL-4 were from Millipore (Billerica, MA) and R&D Systems (Minneapolis, MN), respectively. Krebs–Ringer bicarbonate buffer, DMEM, fatty acid-free (FAF) albumin (FAF-BSA), endotoxin-free FAF-BSA, collagenase A, propidium iodide, Brewer thioglycolate medium, LPS, and PMA were from Sigma (St. Louis, MO). Nylon mesh filters (35 and 100 μm) and mouse BD Fc Block were from BD Biosciences (San Jose, CA). CD11b–allophycocyanin Ab and its isotypic control IgG were from eBioscience (San Diego, CA). F4/80–FITC and its isotypic control IgG were from AbD Serotec (Oxford, U.K.). TRIzol was from Invitrogen (Carlsbad, CA) and L-glutamine from Biological Industries (Kibbutz Beit Haemek, Israel). FBS and Dulbecco´s PBS with ($DPBS^{++}$) and without ($DPBS^{-}$) calcium and magnesium were from Lonza (Verviers, Belgium). HEPES was from Merck (Darmstadt, Germany). Lab-Tek Chamber Slides were from Nalge Nunc International (Rochester, NY). OCT compound was from Sakura Finetek (Tokyo, Japan). FluoSpheres beads of 1 μm and ProLong Gold reagent with DAPI were from Molecular Probes (Eugene, OR). The High-Capacity Archive kit and TaqMan Gene Expression Assays were from Applied Biosystems (Foster City, CA). Protease inhibitor mixture (Complete Mini) and phosphatase inhibitor mixture (PhosSTOP) were from Roche Applied Science (Mannheim, Germany). Phospho–hormone-sensitive lipase (HSL) Ab was from Cell Signaling Technology (Beverly, MA). HRP-linked donkey anti-rabbit Ab was from GE Healthcare (Little Chalfont, U.K.).

Animals and experimental design

Male C57BL/6J mice from Charles River Laboratories (Saint Aubin les Elseuf, France) were housed on wood-chip bedding cages with 50–60% humidity and a 12-h light/dark cycle and given free access to food and water. At 7 wk of age, mice were fed with either standard pelleted chow (TD2014; 13% kcal from fat) or a high-fat diet (HFD) (TD06414; 60% kcal from fat) (Harlan Teklad, Madison, WI). After 12 wk of HFD feeding, obese mice were randomly assigned into two groups receiving (i.p.) either placebo (6%BSA/2.9%EtOH in saline, $n = 17$) or DHA [4 μg/g body weight (b.w.), $n = 20$] every 24 h for 10 d. This dose of DHA was selected based on the actual serum concentrations of nonesterified DHA that mirror the standard intake of ω-3-PUFA supplements (7, 18, 19). At the end of the intervention period, mice were anesthetized (i.p.) with a mixture of 0.1 mg ketamine/g b.w. and 0.01 mg xylazine/g b.w. Blood was collected, and serum was obtained by centrifugation at 800 × *g* for 10 min. Liver was excised, rinsed in $DPBS^{++}$, and placed in OCT, immersed in cold 2-methylbutane on dry ice, and kept at −80°C. Moreover, portions of liver and adipose tissues were snap-frozen in liquid nitrogen for further analysis. Adipose tissue from epididymal fat pads was fixed in 10% formalin and embedded in paraffin or was further processed for adipocyte and stromal vascular cell isolation as described later. All studies were conducted in accordance with the criteria of the Investigation and Ethics Committee of the Hospital Clinic and the European Community laws governing the use of experimental animals.

Biochemical analyses

Serum concentrations of glucose, cholesterol, triglycerides (TAG), and alanine aminotransferase (ALT) were determined by standard laboratory procedures.

Morphometric analysis of adipose tissue sections

Paraffin-embedded epididymal fat pads were cut into 5-μm sections and stained with H&E. For image analysis, six photomicrographs per mouse were randomly obtained under a Nikon Eclipse E600 microscope (Kawasaki, Japan) at ×200 magnification. Adipocyte size was calculated from cross-sectional areas obtained from perimeter tracings using Image J software (Macbiophotonics, McMaster University, Hamilton, ON, Canada).

Detection of F4/80 by immunohistochemistry

F4/80 detection was performed as described previously (20, 21), with slight modifications. Briefly, adipose tissue paraffin sections were deparaffinized, rehydrated, and pretreated with trypsin 0.05%–$CaCl_2$ 0.1% for 20 min at 37°C to unmask the Ag, followed by incubation with 0.3% H_2O_2 for 25 min at room temperature and dark conditions to block endogenous peroxidase activity and with 2% BSA for 20 min at room temperature to avoid unspecific binding of the primary Ab. Sections were then incubated overnight at 4°C with the primary rat anti-mouse F4/80 Ab (1/250), followed by incubation for 30 min at room temperature with a biotinylated rabbit anti-rat IgG secondary Ab (1/200) and incubation with ABC for 30 min at room temperature using Vectastain ABC Kit (Vector, Burlingame, CA). Color was developed using the diaminobenzidine substrate (Roche Diagnostics), and sections were counterstained with hematoxylin. Sections were visualized at magnification ×200 in a Nikon Eclipse E600 microscope (Kawasaki, Japan).

Histological analysis of liver steatosis

Hepatic steatosis was assessed by oil red-O staining in OCT-embedded cryosections. Briefly, sections were fixed in 60% isopropanol for 10 min and stained with 0.3% oil red-O in 60% isopropanol for 30 min and subsequently washed with 60% isopropanol. Sections were counterstained with Gill´s hematoxylin, washed with acetic acid solution (4%), and mounted with aqueous solution. Sections were visualized at a magnification of ×200 in a Nikon Eclipse E600 microscope (Kawasaki, Japan). Relative areas of steatosis (expressed as percent oil red-O staining) were quantified by histomorphometry using a computerized image analysis system (AnalySIS; Soft Imaging System, Munster, Germany). A minimum of 20 independent fields per sample were evaluated.

Detection of secreted proteins by Luminex xMAP technology

IL-6, TNF-α, MCP-1, total plasminogen activator inhibitor-1 (PAI-1), resistin, and leptin protein levels were simultaneously measured in cell culture supernatants using the Milliplex MAP Mouse Adipocyte kit from Millipore. Samples were assayed in duplicate and run on a Luminex 100 Bioanalyzer (Luminex Corp., Austin, TX) according to the kit manufacturer's instructions.

Detection of adiponectin by enzyme immunoassay

Mouse adiponectin levels in serum and adipocyte supernatants were quantified by enzyme immunoassay (Cayman Chemicals).

HSL phosphorylation

Total protein from adipose tissue was extracted in homogenizing buffer containing 50 mM HEPES, 20 mM β-glycerol, 2 mM EDTA, 1% Igepal, 10% glycerol, 1 mM $MgCl_2$, 1 mM $CaCl_2$, 150 mM NaCl, supplemented with protease inhibitor (Complete Mini) and phosphatase inhibitor (PhosSTOP) cocktails. Homogenates were incubated on ice for 15 min with frequent vortexing. Thereafter, homogenates were centrifuged at 16,000 × *g* for 40 min at 4°C, and supernatants were collected. Phospho (Ser-563)-HSL protein expression was analyzed by Western blot. A total of 80 μg protein was resuspended in SDS-containing Laemmli sample buffer, heated for 5 min at 95°C, and resolved on a 10% SDS-PAGE. Proteins were electroblotted for 120 min at 100 V at 4°C onto polyvinyl difluoride

membranes, and the efficiency of the transfer was visualized by Ponceau S solution staining. Membranes were then soaked for 1 h at room temperature in TBS (20 mM Tris/HCl pH 7.4 and 0.5 M NaCl) containing 0.1% (v/v) Tween 20 (0.1% TBST) and 5% (w/v) nonfat dry milk. Blots were washed three times for 5 min each with 0.1% TBST and subsequently treated overnight at 4°C with primary rabbit anti-mouse phospho-HSL Ab (dilution 1:1000) in 0.1% TBST containing 5% BSA. After washing the blots three times for 5 min each with 0.1% TBST, membranes were incubated for 1 h at room temperature with an HRP-linked donkey anti-rabbit secondary Ab (1:2000) in 0.1% TBST. Bands were visualized using the EZ-ECL chemiluminescence detection kit (Biological Industries) in a LAS 4000 imaging system (GE Healthcare Life Sciences) and quantified using Image GE ImageQuant TL analysis software.

Isolation of adipocytes and stromal vascular cells

Epididymal fat pads were excised, weighed, rinsed two times in cold carbogen-gassed Krebs–Ringer, and minced into fine pieces. Minced samples were placed in Krebs–Ringer supplemented with 1% FAF-BSA and 2 mM EDTA and centrifuged at 500 × *g* for 5 min at 4°C to remove free erythrocytes and leukocytes. Tissue suspensions (0.3–0.6 g) were placed in 5 ml digestion buffer containing Krebs–Ringer supplemented with 1% FAF-BSA and 1 mg/ml collagenase A and incubated at 37°C for 30 min with gentle shaking. Tissue homogenates were filtered through a 100-μm nylon mesh and then centrifuged at 500 × *g* for 5 min. Non-digested tissue was further digested for 15 min and filtered as indicated above. Floating cells (adipocytes) were collected, washed two times in carbogen-gassed DMEM supplemented with L-glutamine (2 mM), penicillin (100 U/ml), streptomycin (100 mg/ml), and HEPES (100 mM) and resuspended in DMEM containing L-glutamine (2 mM), penicillin (100 U/ml), streptomycin (100 mg/ml), HEPES (100 mM), and 0.2% endotoxin-free FAF-BSA before counting and plating on 96-well plates. Pelleted cells corresponding with the stromal vascular cells (SVC) were incubated with erythrocyte lysis buffer (0.15 M NH_4Cl, 10 mM $KHCO_3$, and 0.1 mM EDTA) for 5 min, centrifuged at 500 × *g* for 5 min, and filtered through a 35-μm nylon mesh to obtain dissociated cells and resuspended in 0.2% endotoxin-free FAF-BSA DMEM. SVC were plated onto 96-wells for 2 h, and nonadherent cells were removed by two washes with DPBS. The resulting macrophage-enriched SVC were then used for cell incubation experiments.

Cell incubations

Primary adipocytes and SVC from lean and obese animals growing on 96-well plates (50,000 cells/well) were exposed to vehicle (0.1% ethanol), DHA (10, 50, and 100 μM) and arachidonic acid (10 and 50 μM) for 18 h. At the end of the incubation period, culture media was collected under sterile conditions and stored at −20°C for further analysis. Floating adipocytes and attached SVC were resuspended in TRIzol reagent and kept at −80°C for RNA extraction and further gene expression analysis.

Immunophenotyping by flow cytometry

For immunophenotyping experiments, isolated SVC were resuspended in basic sorting buffer ($DPBS^{-/-}$ containing 1 mM EDTA, 25 mM HEPES, pH 7, and 1% FBS), counted, filtered through 35-μm nylon mesh, and prepared for flow cytometry. Briefly, SVC (1.25×10^6 cells/ml) were incubated at 4°C with Mouse BD Fc Block (2.5 μg/ml) prior to staining with fluorescently labeled primary Abs or isotype control IgGs for 50 min at 4°C in the dark. Abs used in these studies included: CD11b–allophycocyanin (0.625 μg/ml) and F4/80–FITC (0.5 μg/ml). After incubation with primary Abs, cell suspensions were washed in 1 ml basic sorting buffer and centrifuged at 500 × *g* for 5 min. Cells were suspended in 0.5 ml basic sorting buffer and analyzed by flow cytometry with a BD FACSCanto II cytometer and FACSDiva v6.1.3 software (BD Biosciences, San Jose, CA). Propidium iodide (4 μg/ml) was used to exclude dead cells. Unstained, single stains, and fluorescence minus one controls were used for setting compensation and gates. The number of double-positive ($CD11b^+/F4/80^+$) cells was normalized to SVC counts and fat weight.

RNA isolation and reverse transcription

Isolation of total RNA from adipose tissue, adipocytes, SVC, and peritoneal macrophages was performed using the TRIzol reagent. RNA concentration was assessed in a NanoDrop-1000 spectrophotometer (NanoDrop Technologies, Wilmington, DE) and its integrity tested on a 6000 LabChip in a Bioanalyzer 2100 (Agilent Technologies, Santa Clara, CA). cDNA synthesis from 200 to 400 ng of total RNA was performed using the High-Capacity cDNA Archive Kit (Applied Biosystems).

Gene expression profiling by PCR and real-time PCR

PCR amplification of 5-LO, 12/15-LO, and GAPDH was performed with specific oligonucleotides (20): 5-LO, sense 5′-CCCCCGAAGCTCCCA-GTGACC-3′ and antisense 5′-TCCCGGGCCTTAGTGTTGATA-3′; 12/15-LO, sense 5′-CCCACCGCCGATTTTCACG-3′ and antisense 5′-AG-TCCTCGCTCAGCCAAGTCATCA-3′; GAPDH, sense 5′-TCCAGTAT-GACTCCACTC-3′ and antisense 5′-ATTTCTCGTGGTTCACAC-3′. The specificity of primers was confirmed in the GenBank database using the basic local alignment search tool and by direct sequencing of the amplified PCR products in an ABI Prism 3130xl Genetic Analyzer using a Big Dye Terminator (version 3.1) Cycle Sequencing Kit (Applied Biosystems). PCR products were analyzed by electrophoresis in 1.5% agarose gels and visualized by ethidium bromide staining using a 100-bp DNA ladder (Invitrogen). For quantification of gene expression by real-time PCR, validated and predesigned TaqMan Gene Expression Assays were used [IL-6 (ID: Mm00446190_m1), TNF-α (ID: Mm00443258_m1), MCP-1 (Ccl2; ID: Mm00441242_m1), peroxisome proliferator-activated receptor γ (Pparg; ID: Mm00440945_m1), IL-10 (ID: Mm00439614_m1), arginase 1 (Arg1; ID: Mm00475988_m1), chitinase-3 like protein (Ym1) (Chi3l3; ID: Mm00657889_mH), mannose receptor C type 1 (CD206) (Mrc1; ID: 00485148_m1), and resistin-like molecule α (RELMα) (Retnla; ID: Mm00445109_m1)], using β-actin (Actb; ID: Mm00607939_s1) as endogenous control. Real-time PCR amplifications were carried out in an Applied Biosystems 7900HT Fast Real Time PCR System. PCR results were analyzed with the Sequence Detector Software version 2.1 (Applied Biosystems). Relative quantification of gene expression was performed using the comparative Ct method. The amount of target gene, normalized to β-actin and relative to a calibrator, was determined by the arithmetic equation $2^{-\Delta\Delta Ct}$ described in the comparative Ct method (User Bulletin #2; http://docs.appliedbiosystems.com/pebiodocs/04303859.pdf).

Isolation of mouse peritoneal macrophages

Both resting and thioglycolate-recruited (3 d after i.p. injection of 2.5 ml 3% thioglycolate) peritoneal macrophages from C57BL/6J mice were collected by peritoneal lavage with 7 ml ice-cold $DPBS^-$. The exudates were centrifuged at 500 × *g* for 5 min and further resuspended in DMEM supplemented with penicillin (100 U/ml), streptomycin (100 μg/ml), 2 mM L-glutamine, and 5% FBS. Cells (120,000 cells/well) were allowed to adhere on 8-well Lab-Tek Chamber Slides or 96-well culture plates over 2 h at 37°C in a humidified 5% CO_2 incubator. Nonadherent cells were removed by washing twice with $DPBS^-$, and the remaining adherent cells were used for the experiments. To assess M1 marker expression profiling, resting cells were exposed to vehicle (0.1% ethanol), IFN-γ (20 ng/ml) plus LPS (100 ng/ml) or IL-4 (20 ng/ml) for 18 h and then incubated for an additional 5 h with resolvin D1 (0.1, 1, 10, and 100 nM), DHA (10, 25, 50, and 100 μM), or IL-4 (20 ng/ml). At the end of the incubation period, medium was removed and macrophages were washed twice and then collected in TRIzol reagent and kept at −80°C for RNA extraction and gene expression analysis.

Phagocytic assay

Thioglycolate-recruited peritoneal macrophages and SVC from obese mice were seeded into 8-well Lab-Tek Chamber Slides in DMEM supplemented with penicillin (100 U/ml), streptomycin (100 μg/ml), 2 mM L-glutamine, and 5% FBS before being treated for 2 h with vehicle (0.1% ethanol), PMA (50 ng/ml), DHA (10, 50, and 100 μM), or resolvin D1 (1, 10, and 100 nM) in the presence of fluorescently labeled latex microspheres (Fluospheres; Molecular Probes). After incubation, unbound particles were removed by washing five times with $DPBS^{++}$. Cells were fixed with 4% paraformaldehyde for 15 min, washed two times with $DPBS^{++}$, and mounted in ProLong Gold antifade reagent with DAPI and visualized at ×630 magnification in a Leica DMI6000B epifluorescence microscope (Leica Microsystems, Wetzlar, Germany). To quantify the number of macrophages containing phagocytosed beads and the number of beads taken up per cell, 10 fields per well were analyzed. Fields were taken randomly, beads and nuclei were counted using Image J software (Macbiophotonics), and the percentage of phagocytic cells and the number of engulfed beads per cell were calculated. Phagocytosis thresholds were established as the percent of phagocytic cells detected under resting conditions.

Reactive oxygen species quantification

Reactive oxygen species (ROS) content in murine peritoneal macrophages was measured using OxiSelect ROS Assay Kit (Cell Biolabs, San Diego, CA) following the manufacturer's instructions. Briefly, attached cells seeded on a black 96-well plate (40,000 cells/well) were pretreated with

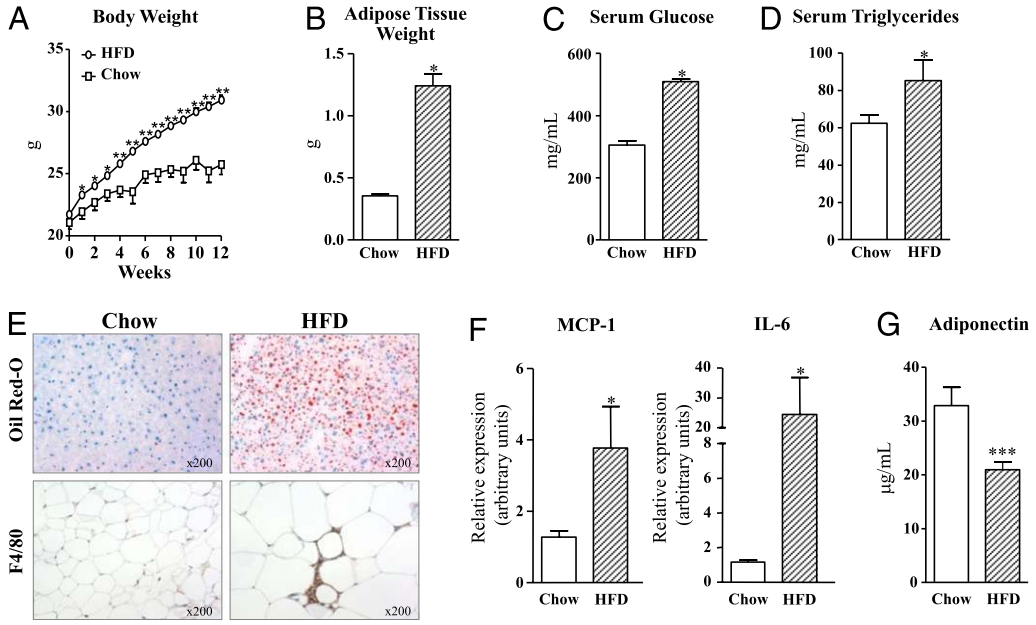

FIGURE 1. HFD-induced obesity accompanied by hepatic steatosis and adipose tissue inflammation. *A–D*, Body weight (*A*), epididymal adipose tissue weight (*B*), serum glucose (*C*), and triglyceride (*D*) levels were measured in mice fed either a chow diet (13% kcal from fat, $n = 13$) or an HFD (60% kcal from fat, $n = 38$) for 12 wk. *E*, Representative photomicrographs (original magnification ×200) of liver sections stained with oil red-O (*upper panels*) and adipose tissue sections stained with F4/80 (*lower panels*) from chow- and HFD-fed animals. *F* and *G*, Adipose tissue MCP-1 and IL-6 gene expression (*F*) and serum adiponectin levels (*G*) in chow- and HFD-fed mice. Results are expressed as mean ± SEM. $*p < 0.05$, $**p < 0.01$, $***p < 0.005$ (versus chow).

vehicle (0.1% ethanol), DHA (10 μM), and resolvin D1 (1 nM) for 2 h in DMEM complete medium. Thereafter, 100 μl of 2′,7′-dichlorofluorescein diacetate probe was added to the wells, and cells were further incubated for 1 h at 37°C. At the end of the incubation period, the medium was removed, and 2′,7′-dichlorofluorescein diacetate–loaded cells were washed twice with $DPBS^{-}$ and stimulated with 50 ng/ml PMA (as an oxidizing agent) in DMEM complete medium. Plates were immediately read at 450-nm excitation and 520-nm emission wavelengths every 5 min for 15 min in a Fluostar Optima fluorescence plate reader (BMG Labtech, Offenburg, Germany).

Statistical analysis of the results was performed using the unpaired Student *t* test. Results were expressed as means ± SE, and differences were considered significant at a *p* value ≤0.05.

Results

To investigate mechanisms underlying adipose tissue inflammation, mice were rendered obese by feeding them an HFD. As anticipated, there were significant differences in b.w., white adipose tissue weight, and serum glucose and TAG levels between lean mice receiving a chow diet (13% kcal from fat) and obese mice receiving an HFD (60% kcal from fat) for 12 wk (Fig. 1*A–D*). In addition, HFD-induced obese mice showed extensive hepatic steatosis (increased staining with oil red-O) and accumulation of macrophages in adipose tissue (increased immunostaining with the F4/80 Ab) (Fig. 1*E*). Increased macrophage infiltration of adipose tissue was also observed in *ob/ob* mice, a genetic model of experimental obesity (Table I). Further evidence for adipose tissue inflammation in HFD-induced obese mice was corroborated by observing a consistent upregulation of the expression of the inflammatory adipokines MCP-1 and IL-6 (Fig. 1*F*). Furthermore, circulating levels of the anti-inflammatory and insulin-sensitizing adipokine adiponectin were significantly reduced in HFD-induced obese mice (Fig. 1*G*).

To test the effects of ω-3-PUFAs on HFD-induced adipose tissue inflammation, obese mice were supplemented with a daily dose of DHA 4 μg/g b.w. for 10 d. No effects on body, liver, and epididymal fat weights and serum cholesterol and ALT levels were observed in DHA-treated mice (Table II). In contrast, serum TAG levels were significantly reduced in obese mice receiving DHA (Table II). Remarkably, DHA alleviated adipose tissue inflammation by downregulating the expression of the inflammatory adipokine MCP-1 (Fig. 2*A*) while increasing the expression of the anti-inflammatory cytokine IL-10 (Fig. 2*B*). Consistent with this amelioration of adipose tissue inflammation, DHA led to significant improvements in serum glucose levels (Fig. 2*C*) and hepatic steatosis, as assessed by oil red-O staining (Fig. 2*D*), in HFD-induced obese mice. To determine whether, in addition to its ability to dampen inflammatory adipokine secretion and steatogenic potential, DHA also modulates other parameters of adipose tissue function, we assessed the effects of this ω-3-PUFA on adipocyte morphometry and on the phosphorylation of HSL, a rate-limiting enzyme of adipocyte lipolysis. As shown in Fig. 2*E* and

Table I. Accumulation of macrophages in adipose tissue samples from two different experimental models of obesity

Parameter	Lean	HFD-Induced Obesity	*ob/ob* Mice
Body weight (g)	27.09 ± 0.52	31.19 ± 0.47[a]	49.45 ± 3.65[a]
Epididymal fat weight (g)	0.34 ± 0.02	1.24 ± 0.09[a]	3.09 ± 0.12[a]
Percentage adipose tissue macrophages (%)	13.8 ± 2.9	26.28 ± 2.67[b]	23.0 ± 0.40[b]

The percentage of adipose tissue macrophages was determined by flow cytometry analysis, as described in *Materials and Methods*.

[a] $p < 0.001$ versus lean mice.

[b] $p < 0.05$ versus lean mice.

Table II. Body, liver, and epididymal fat weights and serum biochemistry values in the three groups of the study

Parameter	Chow (n = 18)	HFD (n = 17)	HFD Plus DHA (n = 18)
Body weight (g)	26.44 ± 0.427	31.19 ± 0.47[a]	30.60 ± 0.54[a]
Liver weight (g)	1.23 ± 0.06	1.21 ± 0.04	1.22 ± 0.04
Epididymal fat weight (g)	0.34 ± 0.02	1.24 ± 0.09[a]	1.18 ± 0.08[a]
Serum cholesterol (mg/dl)	86.6 ± 2.7	134.0 ± 5.6[b]	133.0 ± 3.3[b]
Serum TAG (mg/dl)	62.4 ± 4.3	85.3 ± 11.0[b]	59.4 ± 6.2[c]
Serum ALT (U/l)	40.3 ± 2.7	44.0 ± 6.4	41.1 ± 3.6

[a] $p < 0.005$ versus chow.
[b] $p < 0.05$ versus chow.
[c] $p < 0.05$ versus HFD.

2*F*, DHA did not modify the HFD-induced enlargement of adipocytes or the degree of HFD-induced HSL phosphorylation.

To determine whether the anti-inflammatory properties of DHA in the adipose tissue were related to changes in the population of adipose tissue macrophages, these cells were immunophenotyped by flow cytometry. As expected, mice rendered obese by HFD feeding showed more double-positive CD11b/F4/80 cells, indicative of the presence of a larger number of macrophages in adipose tissue (Fig. 3*A–C*). This finding was confirmed in adipose tissue from obese *ob/ob* mice (data not shown). The administration of DHA to HFD-induced obese mice did not modify either the percentage of double-positive CD11b/F4/80 cells or the absolute number of adipose tissue macrophages (Fig. 3*B*, 3*C*). However, an in-depth analysis of the flow cytometry data revealed that feeding an HFD resulted in an increase in the presence of CD11b^{hi}/F4/80^{hi} macrophages in adipose tissue (Fig. 3*D*). Notably, treatment with DHA inhibited the shift in macrophage F4/80 expression induced by HFD (Fig. 3*D*). Moreover, DHA induced the emergence of a low-expressing CD11b/F4/80 subset of macrophages in the adipose tissue (Fig. 3*E*).

Consistent with the reversal of F4/80^{hi} expression in adipose tissue macrophages, DHA also induced polarization of these cells toward an alternative M2-like activation state. As shown in Fig. 4*A*, the ω-3-PUFA DHA upregulated the expression of recognized established markers of macrophage polarization toward the M2 phenotype, including Arg1, CD206, Ym1, and IL-10, in adipose tissue from HFD-induced obese mice. To confirm that DHA-induced changes in these M2 functional genes were ascribed to macrophages present in the adipose tissue SVC fraction, adipocytes and SVC fractions were isolated from HFD-induced fat pads. As shown in Fig. 4*B*, changes exerted by DHA on IL-10, Arg1, Ym1, and CD206 were specifically confined to the macrophage-enriched SVC fraction. Notably, the M2 marker RELMα was also upregulated by DHA in vivo in SVC from obese mice (Fig. 4*B*). With the exception of a mild change in RELMα expression, no changes were observed in the adipocyte fraction, in which these genes were detected at low or near background levels (Fig. 4*B*).

In addition to upregulating M2 markers, DHA also downregulated the expression of TNF-α and IL-6, two well-established M1

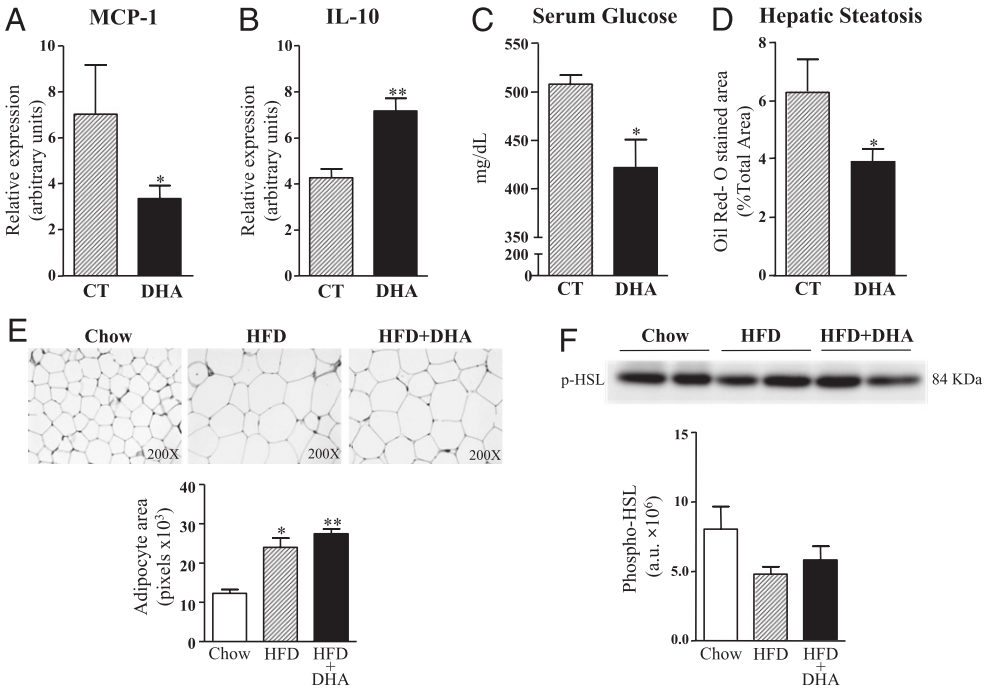

FIGURE 2. Actions of DHA on adipose tissue. *A–D*, Expression of MCP-1 and IL-10 in adipose tissue (*A*, *B*), serum glucose levels (*C*), and hepatic steatosis (*D*) in HFD-induced obese mice treated with either placebo (CT) (6%BSA/2.9%EtOH in saline, n = 17) or DHA (4 μg/g b.w., n = 20) for 10 d. *E*, Morphometric analysis of adipocyte area in adipose tissue sections from mice in chow, HFD, and HFD plus DHA groups. *$p < 0.005$, **$p < 0.001$ (versus chow). *F*, Representative image of p-HSL as determined by Western blot in two consecutive adipose tissue samples from mice in chow, HFD, and HFD plus DHA groups. The densitometric analysis is shown in the *lower panel*.

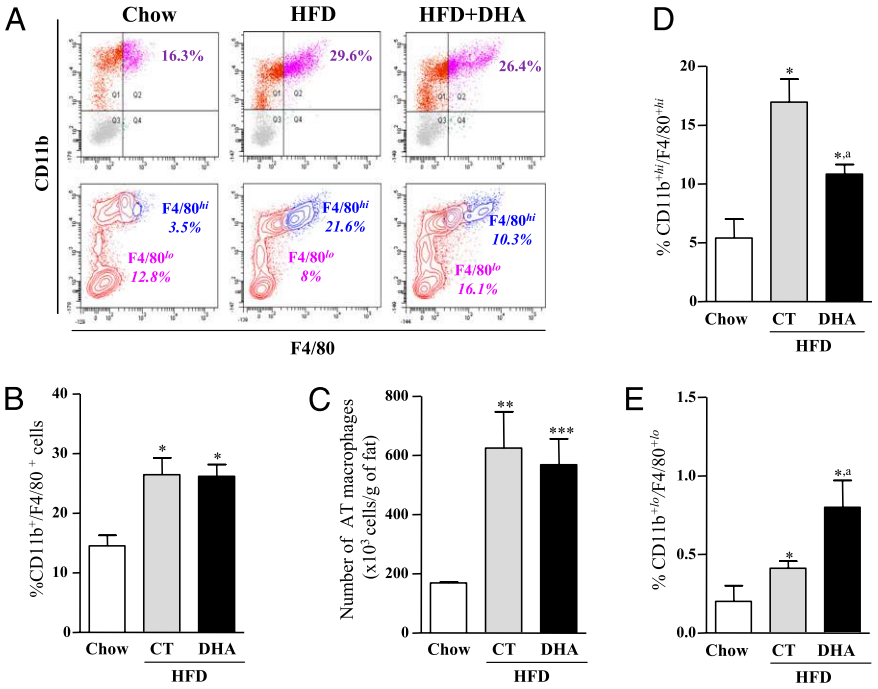

FIGURE 3. Actions of DHA on adipose tissue macrophages. *A*, Analysis by flow cytometry of CD11b and F4/80 marker expression. Adipose tissue SVC isolated from age-matched mice in chow (n = 10), HFD (n = 8), and HFD plus DHA (n = 8) groups were stained with Abs against CD11b and F4/80 and isotype controls and analyzed by flow cytometry using the FACSDiva 6.1.3 software. *Upper panels*, Dot plots from a representative experiment evaluating CD11b and F4/80 expression by SVC. The percentage of double-positive $CD11b^+/F4/80^+$ events is in purple. *Lower panels*, Representative density plots from SVC gated for both double-positive $CD11b^+/F4/80^+$ high (^{hi}; blue gate) and $CD11b^+/F4/80^+$ low (^{lo}; purple gate) expression. The percentage of cells within the $F4/80^{+hi}$ or $F4/80^{+lo}$ macrophage subset is indicated. *B*, Quantification of double-positive cells for CD11b/F4/80 in the three experimental groups of the study. *C*, Absolute number of adipose tissue macrophages in the three groups of the study. The number of double-positive cells was obtained from FACS data and was normalized to total viable SVC and epididymal fat weight. *D*, Flow cytometric analysis of $CD11b^{hi}/F4/80^{hi}$ cell population in viable SVC from the three groups of the study. *E*, Flow cytometric analysis of $CD11b^{lo}/F4/80^{lo}$ cell population in viable SVC from the three groups of the study. Results are expressed as mean ± SEM. *$p < 0.05$, **$p < 0.005$, ***$p < 0.001$ (versus chow), $^a p < 0.05$ (versus HFD).

classically activated macrophage markers (Fig. 5*A*). As expected, the actions of DHA on TNF-α and IL-6 were predominantly ascribed to the macrophage-enriched SVC (Fig. 5*A*). Changes in mRNA expression were confirmed at the protein level by analysis of secreted proteins by Luminex xMAP technology in culture supernatants. As shown in Fig. 5*B*, analysis of the adipokine profile secreted by the separate adipose tissue cell fractions revealed that PAI-1 and MCP-1 are the two most abundant adipokines secreted by adipocytes, whereas MCP-1 and IL-6 are the main adipokines generated in the macrophage-enriched SVC fraction (Fig. 5*B*). Notably, SVC produced significantly higher amounts of TNF-α than those by adipocytes (35.99 ± 9.03 versus 2.04 ± 1.24 pg/ml, $p < 0.05$). Notably, after DHA treatment, there was a significant reduction of the inflammatory adipokines IL-6, MCP-1, and TNF-α in the macrophage-enriched SVC fraction but not in adipocytes, whereas no changes in resistin, total PAI-1, and leptin levels were detected (Fig. 5*C*). Some specific beneficial actions of DHA were also observed in adipocytes, including upregulation of the insulin-sensitizing and anti-inflammatory genes peroxisome proliferator-activated receptor γ (PPARγ) and adiponectin (Fig. 5*D*). The beneficial effects of DHA on PPARγ and adiponectin were found to be concentration-dependent at the micromolar range (Fig. 5*D*, inset). The overall beneficial actions of the ω-3-PUFA DHA on the profile of adipokine secretion were not reproduced by the ω-6-PUFA arachidonic acid (data not shown).

Resolvin D1 is an abundant DHA-derived mediator in adipose tissue from obese mice (7). Resolvin D1 is a member of the recently discovered family of anti-inflammatory autacoids derived from DHA, which biosynthesis in mice involves sequential oxygenation of DHA by 12/15-LO and 5-LO (Fig. 6*A*) (14–16). In our study, we confirmed that the enzymatic machinery required for endogenous resolvin D1 biosynthesis, namely expression of both 12/15-LO and 5-LO, is present in adipose tissue of HFD-induced obese mice (Fig. 6*B*). To determine the actions of this anti-inflammatory mediator on macrophage function, we exposed elicited peritoneal macrophages to synthetic resolvin D1 and compared its effects with those produced by IL-4, a potent anti-inflammatory cytokine. In these experiments, macrophages were classically activated to engage expression of Th1 inflammatory markers by exposure to IFN-γ and LPS. As anticipated, IFN-γ/LPS treatment upregulated the expression of the M1 classically activated macrophage markers TNF-α, MCP-1, and IL-6 (Fig. 6*C*). Remarkably, resolvin D1 attenuated, to a similar extent as IL-4, the expression of TNF-α and IL-6 induced by the exposure of macrophages to IFN-γ and LPS (Fig. 6*C*). Importantly, resolvin D1 significantly reduced TNF-α expression in adipose tissue explants from diet-induced obese mice (0.90 ± 0.09 versus 0.65 ± 0.02 a.u., $p < 0.05$). Similar to IL-4, resolvin D1 failed to prevent IFN-γ/LPS-induced MCP-1 expression (Fig. 6*C*). The resolvin D1 precursor DHA also exerted consistent inhibitory actions on TNF-α, MCP-1, and IL-6 expression (data not shown). In addition to reducing the expression of M1 markers, resolvin D1 increased in a concentration-dependent manner the expression of the functional M2 marker Arg1 in macrophages (Fig. 6*D*, *left panel*). The resolvin D1 precursor DHA also induced Arg1 but at much higher concentrations (Fig. 6*D*, *right panel*). In fact, resolvin D1 was effective in increasing the expression of Arg1 at nanomolar concentrations (ED_{50}: 0.97 nM), whereas DHA exerted significant actions only at the micromolar level (ED_{50}: 3.5 μM). IL-4 was able to induce

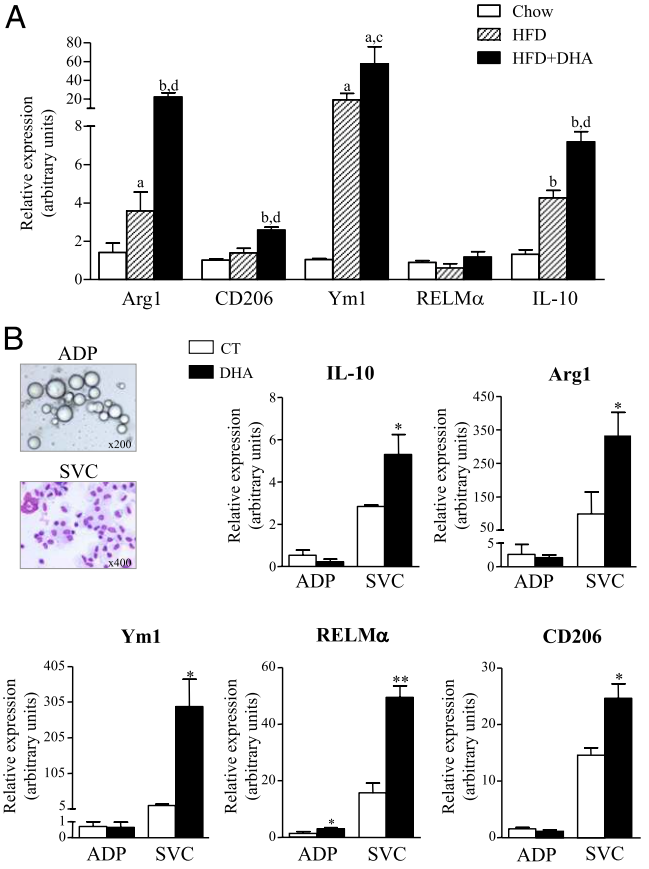

FIGURE 4. The effects of DHA on adipose tissue M2 macrophage markers are confined to the SVC fraction. *A*, Relative mRNA levels of the M2 macrophage markers (Arg1, CD206, Ym1, RELMα, and IL-10) were analyzed by quantitative real-time PCR in adipose tissue from chow, HFD, and HFD plus DHA mice. Results are expressed as the mean ± SEM of six animals per group. $^{a}p < 0.05$, $^{b}p < 0.005$ (versus chow), $^{c}p < 0.05$, $^{d}p < 0.005$ (versus HFD). *B*, Representative photomicrographs of adipocytes (ADP) and SVC fractions and macrophage marker expression in these fractions from HFD mice receiving either placebo (CT) or DHA. Results are expressed as the mean ± SEM, $n = 3$ to 4 per group. $*p < 0.05$, $**p < 0.005$ (versus CT).

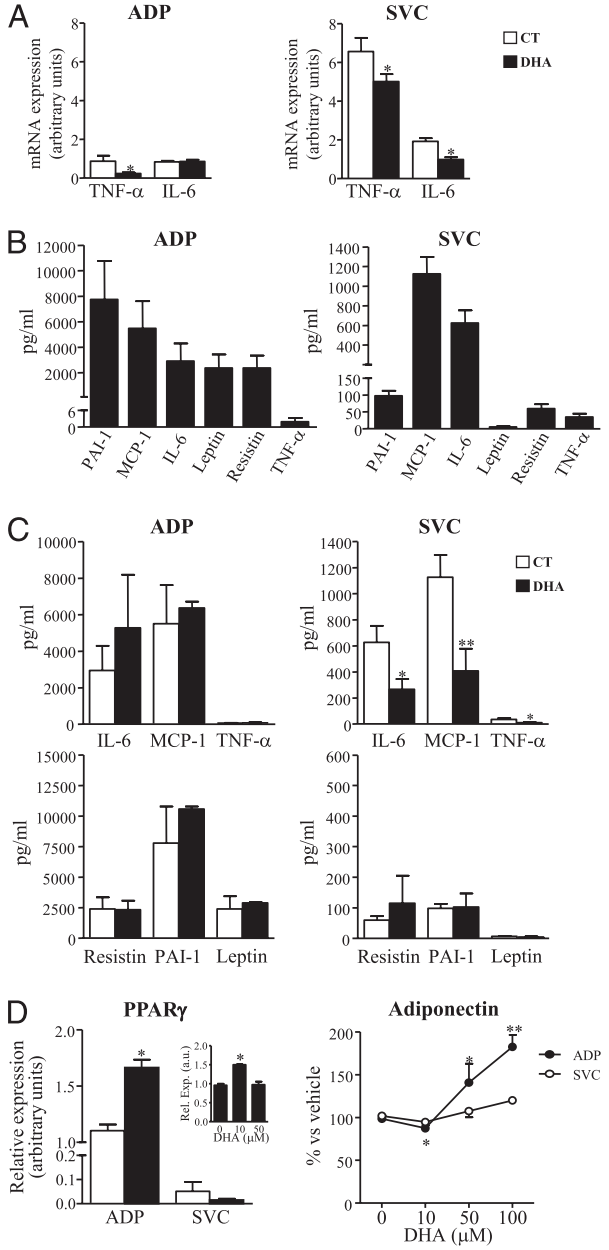

FIGURE 5. DHA regulates the expression and release of Th1 proinflammatory markers and adipokines by adipocytes and SVC. *A*, Relative mRNA levels of the inflammatory Th1 cytokines TNF-α and IL-6 in adipocytes and SVC fractions from HFD-induced obese mice receiving either placebo or DHA. Results are expressed as the mean ± SEM, $n = 3$ to 4 per group. $*p < 0.05$ (versus placebo). *B*, Adipokine profile in supernatants of cultured adipocytes and SVC from HFD mice as detected by xMAP technology (see *Materials and Methods* for details). *C*, Adipokine levels in supernatants of cultured adipocytes and SVC from HFD-induced obese mice receiving either placebo or DHA. Results are expressed as the mean ± SEM, $n = 3$ to 6 per group. $*p < 0.05$, $**p < 0.01$ (versus placebo). *D*, Concentration-dependent effects of DHA on PPARγ mRNA expression and adiponectin release by adipocytes and SVC from HFD mice receiving placebo (empty bars) or DHA (solid bars). Adiponectin results are presented as percentage of production compared with vehicle. Results are expressed as the mean ± SEM of three to six experiments assayed in duplicate. $*p < 0.05$, $**p < 0.01$ (versus placebo or vehicle). ADP, adipocytes; CT, placebo.

both Arg1 and Ym1 (Fig. 6*D*, *middle panel*). No changes in CD206 and RELMα were detected in macrophages exposed to either resolvin D1 or DHA (data not shown). Most notably, these effects were confirmed in adipose tissue macrophages from the SVC fraction of obese mice (data not shown).

To gain a better insight into the effects of resolvin D1 on macrophage function, we exposed elicited peritoneal macrophages to resolvin D1 and assessed its effects on macrophage phagocytosis. As shown in Fig. 7*A* and 7*B*, resolvin D1 was a very potent inducer of macrophage phagocytosis, as this lipid autacoid induced in a concentration-dependent manner both the number of macrophages containing phagocytosed beads and the number of internalized beads per cell. Unexpectedly, the resolvin D1 precursor DHA exerted an opposite effect to that of resolvin D1 and significantly reduced macrophage phagocytic activity (Fig. 7*A*, 7*B*). Importantly, resolvin D1, but not its precursor DHA, enhanced the phagocytic activity of macrophages from the adipose tissue SVC fraction (Fig. 7*C*). Finally and because ROS production is linked to classical macrophage activation, a fluorogenic assay was performed in the presence or absence of resolvin D1 and DHA. As shown in Fig. 7*D*, resolvin D1 treatment attenuated ROS production by macrophages in response to PMA, an effect that was not observed with DHA. Collectively, these findings establish resolvin D1 as an activator of nonphlogistic phagocytosis in macrophages, which is an essential step for the resolution of the inflammatory response.

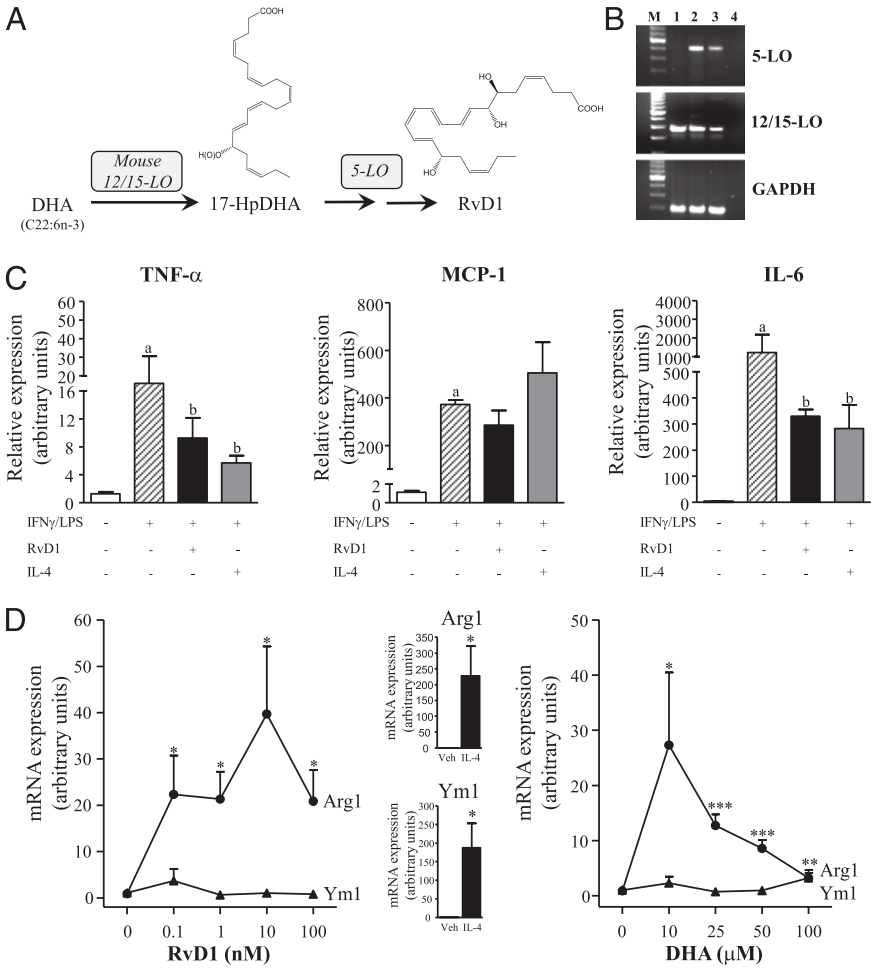

FIGURE 6. Resolvin D1 potently attenuates M1 inflammatory markers while increasing the functional M2 macrophage marker Arg1. *A*, Enzymatic pathway for resolvin D1 biosynthesis. Resolvins of the D series are endogenously produced through the action of 15-LO (12/15-LO in the mouse), which converts DHA into 17*S*-hydro (peroxy) DHA (17-HpDHA). Subsequently, 17-HpDHA is rapidly converted into resolvin D1 by 5-LO. *B*, Representative PCR analysis of mRNA expression for 5-LO, 12/15-LO, and GAPDH in adipose tissue from mice fed chow (*lane 1*) or HFD (*lane 2*). *Lanes 3* (Raw 264.7 cells) and *4* (water) were used as positive and negative controls, respectively. A 100-bp DNA ladder was used as a size standard (M). *C*, Expression of M1 inflammatory markers in peritoneal macrophages. Macrophages from lean mice were exposed to vehicle (0.2% sodium phosphate, 5 mM) or IFN-γ/LPS (IFN-γ 20 ng/ml, LPS 100 ng/ml) for 18 h and then incubated for 5 h with vehicle (0.5% ethanol), resolvin D1 (10 nM), or IL-4 (20 ng/ml). $^{a}p <$ 0.05 (versus vehicle), $^{b}p < 0.05$ (versus IFN-γ/LPS treatment). *D*, Changes in the expression of the M2 macrophage markers Arg1 and Ym1 to increasing concentrations of resolvin D1 and DHA. The response to IL-4 (20 ng/ml) is shown in the *middle panel*. $*p < 0.05$, $**p <$ 0.001, $***p < 0.0001$ (versus vehicle). RvD1, resolvin D1.

Discussion

Tissue macrophages are phenotypically heterogeneous and are broadly characterized according to their activation (polarization) state (22, 23). Using a well-established model of dietary obesity, in the current study we demonstrate that the ω-3-PUFA DHA switches adipose tissue-infiltrating macrophages from a dominant inflammatory M1 classically activated phenotype toward an alternative activated M2-like phenotype. Notably, in this study we demonstrate that resolvin D1, a potent anti-inflammatory lipid mediator derived from DHA, can skew macrophages from the M1 phenotype and hence promote the resolution of chronic adipose tissue inflammation associated with obesity. These findings are consistent with the "phenotype switch" model proposed by Lumeng and others (24–26) in which recruited adipose tissue macrophages in obesity have an activation pattern similar to M1-polarized macrophages. Moreover, our flow cytometry data are in agreement with the presence of a predominant low-expressing F4/80 (F4/80^{lo}) macrophage subset in lean mice and its shift to F4/80^{hi} macrophages favoring a predominance of M1 markers in adipose tissue of obese mice, as initially described by Bassaganya-Riera et al. (27). Notably, our findings are in line with those reported by Schif-Zuck et al. (28), who demonstrated the emergence of a proresolving population of macrophages that express low levels of CD11b during the resolution of murine peritonitis. Collectively, our study supports the notion that polarization of macrophages toward an M2-like phenotype is essential for resolution of inflammation and complete homeostasis of adipose tissue.

Resolution of inflammation is not a mere passive process of dilution of inflammation but is rather a highly orchestrated and complex process in which endogenously generated anti-inflammatory and proresolving mediators counteract the effects of proinflammatory signaling systems (29). Resolvins are a new paradigm of these endogenous mediators that promote resolution of inflammation and stimulate the return to homeostasis (11, 12). These novel chemical mediators are classified as either resolvin E1 if the biosynthesis is initiated from eicosapentaenoic acid or resolvin D1 if they are generated from DHA (11, 12). Resolvins regulate receptor-mediated intracellular signaling pathways in target tissues leading to potent anti-inflammatory and proresolution properties (30–35). Resolvin E1, in particular, decreases PMN infiltration and T cell migration, reduces TNF-α and IFN-γ secretion, inhibits chemokine formation, and blocks IL-1–induced NF-κB activation (30–34). In vivo, resolvin E1 exerts potent anti-inflammatory actions in experimental models of periodontitis, colitis, and peritonitis and protects mice against brain ischemia–reperfusion (30–34). In a genetic model of obesity, resolvin E1 has shown significant insulin-sensitizing effects by upregulating adiponectin, GLUT-4, insulin receptor substrate-1, and PPARγ expression in the adipose tissue and has been shown to confer significant protection against hepatic steatosis (7). In the current study, we specifically focused on the actions of resolvin D1, because this anti-inflammatory and proresolving mediator is abundant in adipose tissue from obese mice (7). Resolvin D1, which is biosynthesized from DHA via 15-LO–5-LO interactions, limits PMN infiltration and oxidative stress while enhancing macrophage phagocytosis and clearance of apoptotic cells and microbes (14–17).

In this study, we provide evidence that resolvin D1 skews macrophages from predominantly expressing inflammatory genes such

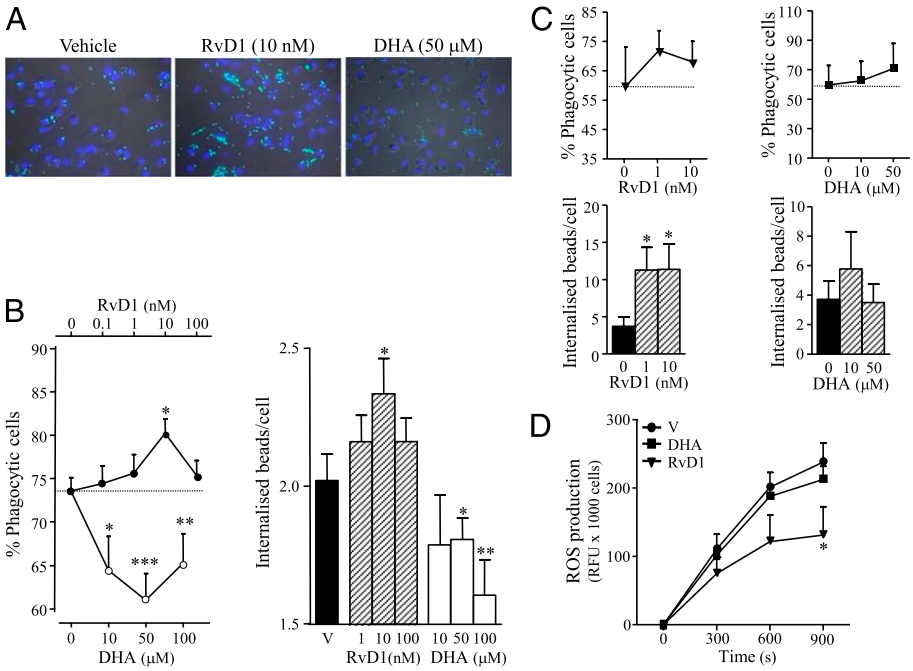

FIGURE 7. Resolvin D1 stimulates non-phlogistic macrophage phagocytosis. *A*, Representative images of fluorescently labeled latex microspheres engulfed by thioglycolate-elicited peritoneal macrophages incubated for 2 h with vehicle (0.1% ethanol), resolvin D1 (10 nM), or DHA (50 μM). Images were taken using an epifluorescent microscope (original magnification ×630). Nuclei were stained with DAPI and ingested beads with yellow-green label. *B*, Quantification of percentage of phagocytic cells (cells containing phagocytosed beads) and the number of beads taken per cell in macrophages incubated for 2 h with vehicle (V, 0.1% ethanol), resolvin D1 (0.1, 1, 10, and 100 nM), or DHA (10, 50, and 100 μM). The dotted line indicates the phagocytosis threshold, established as the percentage of phagocytic cells detected under resting conditions. Quantification was performed using Image J software as described in *Materials and Methods*. *C*, The phagocytosis assay was performed in adipose tissue SVC macrophages as described in *B*. *D*, ROS production kinetics was measured in thioglycolate-elicited peritoneal macrophages exposed to vehicle (V, 0.1% ethanol), resolvin D1 (1 nM), or DHA (10 μM) as described in *Materials and Methods*. Results represent the mean ± SEM of three to five experiments assayed in duplicate. $*p < 0.05$, $**p < 0.005$, $***p < 0.0001$ (versus V or time 0). RvD1, resolvin D1.

as TNF-α and IL-6. In fact, resolvin D1 was as effective as the Th2 cytokine IL-4 at inhibiting inflammatory cytokine production and at conferring an M2-like anti-inflammatory phenotype to macrophages. Importantly, administration in vivo of the resolvin D1 precursor DHA induced the expression in adipose tissue of the M2 markers IL-10, Arg1, the chitinase family member Ym1, RELMα, and the C-type lectin receptor CD206, widely known as the mannose receptor. Consistent with this, administration in vitro of synthetic resolvin D1 to macrophages in culture specifically increased Arg1 expression, which in the current paradigm of macrophage polarization is a functional hallmark of M2 macrophages (36). Arg1 and inducible NO synthase (iNOS) both use L-arginine as substrate, but whereas iNOS generates reactive NO species with proinflammatory actions, Arg1 competes with iNOS for L-arginine and generates L-ornithine, a precursor for proline that enhances collagen biosynthesis (37). This balance in favor of Arg1 may play a critical role in repressing ROS and thus promoting resolution of the inflammatory response, tissue repair, and remodeling. In fact, in our experiments resolvin D1 consistently stimulated in a concentration-dependent manner macrophage phagocytosis, a primary effector function of M2 macrophages important for limiting the inflammatory response. It is noteworthy to mention the observed dissociation between the actions of resolvin D1 and its precursor DHA on the phagocytic activity of both peritoneal and adipose SVC macrophages. Notably, the resolvin D1-enhanced effector function of macrophages was not accompanied by an increase in ROS generation in PMA-elicited peritoneal macrophages. This is an important observation because in contrast to the inflammatory response triggered by an infection in which ROS generation and microorganism killing are essential, resolution of adipose tissue inflammation is a process that involves immune-silencing of macrophages to prevent chronic inflammation and inappropriate tissue damage (32).

Because the presence of uncontrolled inflammation in adipose tissue plays a major role in the development of obesity-related complications such as insulin resistance, type 2 diabetes, and non-alcoholic fatty liver disease, any strategy aimed to disrupt the sequence of events leading to the chronic "low-grade" inflammatory state in this tissue would be beneficial. One such strategy to combat inflammation in adipose tissue is based on the awareness of the unequivocal health benefits of ω-3-PUFAs (7–10). This notion is well supported by the following observations: 1) adipose tissue represents the main storage site of ω-3-PUFAs in obese individuals (38); 2) ω-3-PUFA supplementation produces additive benefits on insulin sensitivity, lipid profile, and inflammation during the management of weight loss in overweight hyperinsulinemic women (39); 3) intake of an ω-3-PUFA–enriched diet significantly alleviates insulin resistance and hepatic steatosis in obese *ob/ob* mice (7); 4) mice with transgenic expression of the ω-3 fatty acid desaturase (*fat-1*), which endogenously enriches tissues with ω-3-PUFAs, display improved glucose tolerance and reduced b.w. (40); and 5) dietary deprivation of ω-3-PUFAs, in contrast, induces changes in tissue fatty acid composition leading to severe metabolic alterations such as augmented adipose tissue mass and plasma glucose, decreased insulin sensitivity, and hepatic steatosis (41, 42). It is important to note that in our study, not all adipose tissue functions were positively modulated by the ω-3-PUFA DHA. For instance, DHA was ineffective in reducing HFD-induced adipocyte enlargement and HSL phosphorylation, which is a rate-limiting enzyme in adipose tissue lipolysis, suggesting

that the observed hepatic antisteatotic actions of DHA are not the direct consequence of an improvement in circulating levels of free fatty acids. It could be speculated, therefore, that the beneficial actions of DHA on fatty liver disease are related to the reduction in the release of prosteatotic and inflammatory adipokines by adipose tissue (i.e., TNF-α and IL-6) or by direct effects of this ω-3-PUFA on the liver (43). Finally, our study also helps to shed some light on the enduring question of which would be the best option for promoting the timely resolution of inflamed fat tissue in obesity: supplementation of ω-3-PUFAs in the diet or administration of the novel ω-3–derived mediators (i.e., resolvin D1). In this regard, the finding that resolvin D1 exerts anti-inflammatory properties at nanomolar concentrations, whereas its precursor DHA is only effective at the micromolar level, supports the view that resolvins could be an effective and safe alternative for combating inflammation in obesity. In fact, a recent study by Hellman et al. (44) provides solid evidence that resolvin D1 can effectively improve insulin sensitivity in obese-diabetic mice.

In summary, the findings of this study demonstrate that resolvin D1 and its precursor DHA produce a functional switch in adipose tissue macrophage polarization toward an M2-like phenotype in obese mice. Our findings also indicate that the macrophage regulatory properties of resolvin D1 may account for its protective actions against obesity-induced adipose tissue inflammation, insulin resistance, and metabolic liver disease.

Acknowledgments

We thank Isabel Crespo for assistance with flow cytometry experiments at the Flow Cytometry Unit of the August Pi i Sunyer Biomedical Research Institute. We also thank Dr. Josefina López-Aguilar and Elisa Quilez from the Corporació Sanitària Parc Taulí for technical support in the use of the Luminex 100 Bioanalyzer.

Disclosures

The authors have no financial conflicts of interest.

References

1. Ferrante, A. W., Jr. 2007. Obesity-induced inflammation: a metabolic dialogue in the language of inflammation. *J. Intern. Med.* 262: 408–414.
2. Gustafson, B. 2010. Adipose tissue, inflammation and atherosclerosis. *J. Atheroscler. Thromb.* 17: 332–341.
3. Weisberg, S. P., D. McCann, M. Desai, M. Rosenbaum, R. L. Leibel, and A. W. Ferrante, Jr. 2003. Obesity is associated with macrophage accumulation in adipose tissue. *J. Clin. Invest.* 112: 1796–1808.
4. Xu, H., G. T. Barnes, Q. Yang, G. Tan, D. Yang, C. J. Chou, J. Sole, A. Nichols, J. S. Ross, L. A. Tartaglia, and H. Chen. 2003. Chronic inflammation in fat plays a crucial role in the development of obesity-related insulin resistance. *J. Clin. Invest.* 112: 1821–1830.
5. Wellen, K. E., and G. S. Hotamisligil. 2003. Obesity-induced inflammatory changes in adipose tissue. *J. Clin. Invest.* 112: 1785–1788.
6. Cancello, R., C. Henegar, N. Viguerie, S. Taleb, C. Poitou, C. Rouault, M. Coupaye, V. Pelloux, D. Hugol, J. L. Bouillot, et al. 2005. Reduction of macrophage infiltration and chemoattractant gene expression changes in white adipose tissue of morbidly obese subjects after surgery-induced weight loss. *Diabetes* 54: 2277–2286.
7. González-Périz, A., R. Horrillo, N. Ferré, K. Gronert, B. Dong, E. Morán-Salvador, E. Titos, M. Martínez-Clemente, M. López-Parra, V. Arroyo, and J. Clària. 2009. Obesity-induced insulin resistance and hepatic steatosis are alleviated by omega-3 fatty acids: a role for resolvins and protectins. *FASEB J.* 23: 1946–1957.
8. Kopecky, J., M. Rossmeisl, P. Flachs, O. Kuda, P. Brauner, Z. Jilkova, B. Stankova, E. Tvrzicka, and M. Bryhn. 2009. n-3 PUFA: bioavailability and modulation of adipose tissue function. *Proc. Nutr. Soc.* 68: 361–369.
9. Huber, J., M. Löffler, M. Bilban, M. Reimers, A. Kadl, J. Todoric, M. Zeyda, R. Geyeregger, M. Schreiner, T. Weichhart, et al. 2007. Prevention of high-fat diet-induced adipose tissue remodeling in obese diabetic mice by n-3 polyunsaturated fatty acids. *Int J Obes (Lond)* 31: 1004–1013.
10. Todoric, J., M. Löffler, J. Huber, M. Bilban, M. Reimers, A. Kadl, M. Zeyda, W. Waldhäusl, and T. M. Stulnig. 2006. Adipose tissue inflammation induced by high-fat diet in obese diabetic mice is prevented by n-3 polyunsaturated fatty acids. *Diabetologia* 49: 2109–2119.
11. Bannenberg, G., and C. N. Serhan. 2010. Specialized pro-resolving lipid mediators in the inflammatory response: An update. *Biochim. Biophys. Acta* 1801: 1260–1273.
12. Serhan, C. N., N. Chiang, and T. E. Van Dyke. 2008. Resolving inflammation: dual anti-inflammatory and pro-resolution lipid mediators. *Nat. Rev. Immunol.* 8: 349–361.
13. Serhan, C. N., S. Hong, K. Gronert, S. P. Colgan, P. R. Devchand, G. Mirick, and R. L. Moussignac. 2002. Resolvins: a family of bioactive products of omega-3 fatty acid transformation circuits initiated by aspirin treatment that counter proinflammation signals. *J. Exp. Med.* 196: 1025–1037.
14. Hong, S., K. Gronert, P. R. Devchand, R. L. Moussignac, and C. N. Serhan. 2003. Novel docosatrienes and 17S-resolvins generated from docosahexaenoic acid in murine brain, human blood, and glial cells. Autacoids in anti-inflammation. *J. Biol. Chem.* 278: 14677–14687.
15. Krishnamoorthy, S., A. Recchiuti, N. Chiang, S. Yacoubian, C. H. Lee, R. Yang, N. A. Petasis, and C. N. Serhan. 2010. Resolvin D1 binds human phagocytes with evidence for proresolving receptors. *Proc. Natl. Acad. Sci. USA* 107: 1660–1665.
16. Spite, M., L. Summers, T. F. Porter, S. Srivastava, A. Bhatnagar, and C. N. Serhan. 2009. Resolvin D1 controls inflammation initiated by glutathione-lipid conjugates formed during oxidative stress. *Br. J. Pharmacol.* 158: 1062–1073.
17. Sun, Y. P., S. F. Oh, J. Uddin, R. Yang, K. Gotlinger, E. Campbell, S. P. Colgan, N. A. Petasis, and C. N. Serhan. 2007. Resolvin D1 and its aspirin-triggered 17R epimer. Stereochemical assignments, anti-inflammatory properties, and enzymatic inactivation. *J. Biol. Chem.* 282: 9323–9334.
18. Kielar, M. L., D. R. Jeyarajah, X. J. Zhou, and C. Y. Lu. 2003. Docosahexaenoic acid ameliorates murine ischemic acute renal failure and prevents increases in mRNA abundance for both TNF-alpha and inducible nitric oxide synthase. *J. Am. Soc. Nephrol.* 14: 389–396.
19. Delorme, J., C. Benassayag, N. Christeff, G. Vallette, L. Savu, and E. Nunez. 1984. Age-dependent responses of the serum non-esterified fatty acids to adrenalectomy and ovariectomy in developing rats. *Biochim. Biophys. Acta* 792: 6–10.
20. Horrillo, R., A. González-Périz, M. Martínez-Clemente, M. López-Parra, N. Ferré, E. Titos, E. Morán-Salvador, R. Deulofeu, V. Arroyo, and J. Clària. 2010. 5-lipoxygenase activating protein signals adipose tissue inflammation and lipid dysfunction in experimental obesity. *J. Immunol.* 184: 3978–3987.
21. Martínez-Clemente, M., N. Ferré, E. Titos, R. Horrillo, A. González-Périz, E. Morán-Salvador, C. López-Vicario, R. Miquel, V. Arroyo, C. D. Funk, and J. Clària. 2010. Disruption of the 12/15-lipoxygenase gene (Alox15) protects hyperlipidemic mice from nonalcoholic fatty liver disease. *Hepatology* 52: 1980–1991.
22. Martínez, F. O., L. Helming, and S. Gordon. 2009. Alternative activation of macrophages: an immunologic functional perspective. *Annu. Rev. Immunol.* 27: 451–483.
23. Bystrom, J., I. Evans, J. Newson, M. Stables, I. Toor, N. van Rooijen, M. Crawford, P. Colville-Nash, S. Farrow, and D. W. Gilroy. 2008. Resolution-phase macrophages possess a unique inflammatory phenotype that is controlled by cAMP. *Blood* 112: 4117–4127.
24. Lumeng, C. N., J. L. Bodzin, and A. R. Saltiel. 2007. Obesity induces a phenotypic switch in adipose tissue macrophage polarization. *J. Clin. Invest.* 117: 175–184.
25. Lumeng, C. N., J. B. DelProposto, D. J. Westcott, and A. R. Saltiel. 2008. Phenotypic switching of adipose tissue macrophages with obesity is generated by spatiotemporal differences in macrophage subtypes. *Diabetes* 57: 3239–3246.
26. Shaul, M. E., G. Bennett, K. J. Strissel, A. S. Greenberg, and M. S. Obin. 2010. Dynamic, M2-like remodeling phenotypes of CD11c+ adipose tissue macrophages during high-fat diet—induced obesity in mice. *Diabetes* 59: 1171–1181.
27. Bassaganya-Riera, J., S. Misyak, A. J. Guri, and R. Hontecillas. 2009. PPAR gamma is highly expressed in F4/80(hi) adipose tissue macrophages and dampens adipose-tissue inflammation. *Cell. Immunol.* 258: 138–146.
28. Schif-Zuck, S., N. Gross, S. Assi, R. Rostoker, C. N. Serhan, and A. Ariel. 2011. Saturated-efferocytosis generates pro-resolving CD11b low macrophages: modulation by resolvins and glucocorticoids. *Eur. J. Immunol.* 41: 366–379.
29. Serhan, C. N., S. D. Brain, C. D. Buckley, D. W. Gilroy, C. Haslett, L. A. O'Neill, M. Perretti, A. G. Rossi, and J. L. Wallace. 2007. Resolution of inflammation: state of the art, definitions and terms. *FASEB J.* 21: 325–332.
30. Arita, M., F. Bianchini, J. Aliberti, A. Sher, N. Chiang, S. Hong, R. Yang, N. A. Petasis, and C. N. Serhan. 2005. Stereochemical assignment, antiinflammatory properties, and receptor for the omega-3 lipid mediator resolvin E1. *J. Exp. Med.* 201: 713–722.
31. Arita, M., M. Yoshida, S. Hong, E. Tjonahen, J. N. Glickman, N. A. Petasis, R. S. Blumberg, and C. N. Serhan. 2005. Resolvin E1, an endogenous lipid mediator derived from omega-3 eicosapentaenoic acid, protects against 2,4,6-trinitrobenzene sulfonic acid-induced colitis. *Proc. Natl. Acad. Sci. USA* 102: 7671–7676.
32. Haas-Stapleton, E. J., Y. Lu, S. Hong, M. Arita, S. Favoreto, S. Nigam, C. N. Serhan, and N. Agabian. 2007. *Candida albicans* modulates host defense by biosynthesizing the pro-resolving mediator resolvin E1. *PLoS ONE* 2: e1316.
33. Schwab, J. M., N. Chiang, M. Arita, and C. N. Serhan. 2007. Resolvin E1 and protectin D1 activate inflammation-resolution programmes. *Nature* 447: 869–874.
34. Haworth, O., M. Cernadas, R. Yang, C. N. Serhan, and B. D. Levy. 2008. Resolvin E1 regulates interleukin 23, interferon-gamma and lipoxin A4 to promote the resolution of allergic airway inflammation. *Nat. Immunol.* 9: 873–879.
35. Spite, M., L. V. Norling, L. Summers, R. Yang, D. Cooper, N. A. Petasis, R. J. Flower, M. Perretti, and C. N. Serhan. 2009. Resolvin D2 is a potent regulator of leukocytes and controls microbial sepsis. *Nature* 461: 1287–1291.

36. Gordon, S. 2003. Alternative activation of macrophages. *Nat. Rev. Immunol.* 3: 23–35.
37. Bronte, V., and P. Zanovello. 2005. Regulation of immune responses by L-arginine metabolism. *Nat. Rev. Immunol.* 5: 641–654.
38. Lundbom, J., S. Heikkinen, B. Fielding, A. Hakkarainen, M. R. Taskinen, and N. Lundbom. 2009. PRESS echo time behavior of triglyceride resonances at 1.5T: detecting omega-3 fatty acids in adipose tissue in vivo. *J. Magn. Reson.* 201: 39–47.
39. Krebs, J. D., L. M. Browning, N. K. McLean, J. L. Rothwell, G. D. Mishra, C. S. Moore, and S. A. Jebb. 2006. Additive benefits of long-chain n-3 polyunsaturated fatty acids and weight-loss in the management of cardiovascular disease risk in overweight hyperinsulinaemic women. *Int J Obes (Lond)* 30: 1535–1544.
40. Ji, S., R. W. Hardy, and P. A. Wood. 2009. Transgenic expression of n-3 fatty acid desaturase (fat-1) in C57/BL6 mice: effects on glucose homeostasis and body weight. *J. Cell. Biochem.* 107: 809–817.
41. Pachikian, B. D., A. M. Neyrinck, P. D. Cani, L. Portois, L. Deldicque, F. C. De Backer, L. B. Bindels, F. M. Sohet, W. J. Malaisse, M. Francaux, et al. 2008. Hepatic steatosis in n-3 fatty acid depleted mice: focus on metabolic alterations related to tissue fatty acid composition. *BMC Physiol.* 8: 21.
42. Sener, A., Y. Zhang, N. Bulur, K. Louchami, W. J. Malaisse, and Y. A. Carpentier. 2009. The metabolic syndrome of omega3-depleted rats. II. Body weight, adipose tissue mass and glycemic homeostasis. *Int. J. Mol. Med.* 24: 125–129.
43. González-Périz, A., A. Planagumà, K. Gronert, R. Miquel, M. López-Parra, E. Titos, R. Horrillo, N. Ferré, R. Deulofeu, V. Arroyo, et al. 2006. Docosahexaenoic acid (DHA) blunts liver injury by conversion to protective lipid mediators: protectin D1 and 17S-hydroxy-DHA. *FASEB J.* 20: 2537–2539.
44. Hellmann, J., Y. Tang, M. Kosuri, A. Bhatnagar, and M. Spite. 2011. Resolvin D1 decreases adipose tissue macrophage accumulation and improves insulin sensitivity in obese-diabetic mice. *FASEB J.* 25: 2399–2407.